Electronic Supplementary Material (ESI)

Ancient pigment to treasure: Prussian blue as a cheap solid cyanide/nitrogen dual-source affording high-yield syntheses of pricey endohedral clusterfullerenes

Jinpeng Xin,[a,†] Fei Jin,[a,†] Runnan Guan,[a] Muqing Chen,[a] Xiao-Ming Xie,[b] Qianyan Zhang,*[b] Su-Yuan Xie,[b] and Shangfeng Yang*[a]

[a] Hefei National Laboratory for Physical Sciences at Microscale, CAS Key Laboratory of Materials for Energy Conversion, Department of Materials Science and Engineering, Synergetic Innovation Center of Quantum Information & Quantum Physics, University of Science and Technology of China, Hefei 230026, China

[b] State Key Lab for Physical Chemistry of Solid Surfaces, Collaborative Innovation Center of Chemistry for Energy Materials, Department of Chemistry, College of Chemistry and Chemical Engineering, Xiamen University, Xiamen 361005, China

Table of Contents

S1. Isolation and Estimation of the relative yields of DyCN@C_{82} (C_2(5), C_s(6), C_{2v}(9)).

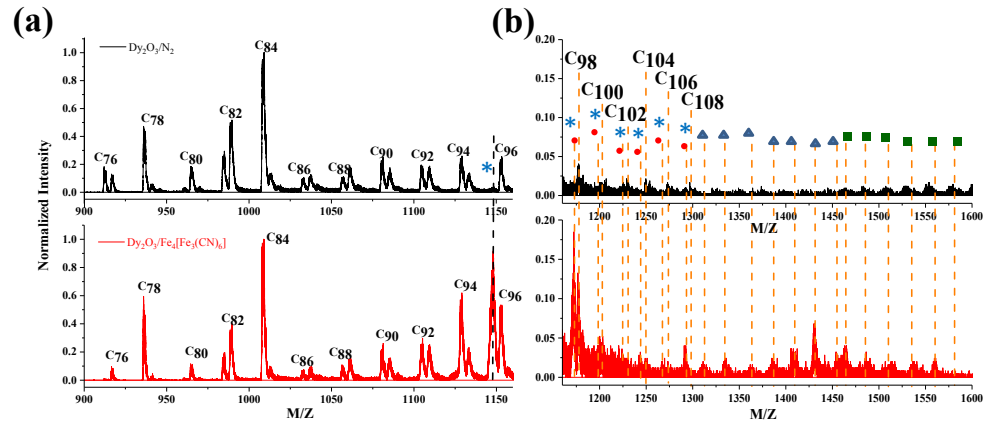

Fig. S1. MALDI-TOF mass spectra of the HPLC fractions obtained from Dy_2O_3/N_2 and $Dy_2O_3/Fe_4[Fe(CN)_6]_3$ extracts with retention time longer than 12 min. (**a**) Spectra in the M/Z range of 900 - 1160; (**b**) Spectra in the M/Z range of 1160 - 1600. * indicates $Dy@C_{2n}$ (n=41-53); ▲ indicates Dy_2C_{2n} (n=41-47); ● indicates $DyCN@C_{2n}$ (2n=41-46); ■ indicates $Dy_3N@C_{2n}$ (n=40-45).

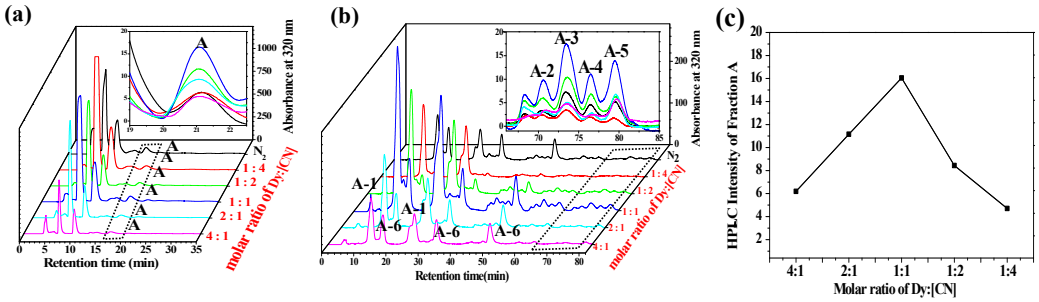

Fig. S2. HPLC chromatograms of $Dy_2O_3/Fe_4[Fe(CN)_6]_3$ extracts with different Dy:[CN] molar ratios and HPLC intensity of fraction A. (**a**) HPLC chromatograms of $Dy_2O_3/Fe_4[Fe(CN)_6]_3$ fullerene extracts with different Dy:[CN] molar ratios (20 mm×250 mm 5PYE column; flow rate 15.0 mL min^{-1}; injection volume 15 mL; toluene as the eluent (mobile phase); 40 °C). The dotted rhombus marks the enlarged region containing fraction **A**. Inset: the enlarged region of retention time ranging from 19 to 23 min. (**b**) Recycling HPLC chromatograms of fraction **A** obtained with different Dy:[CN] molar ratios (10 mm×250 mm BPM column; flow rate 5.0 mL min^{-1}; injection volume 5 mL; toluene as the eluent (mobile phase); 40 °C). The dotted rhombus marks the enlarged region containing subfractions **A-2** to **A-6** shown in the inset of Fig. 2c. Inset: the enlarged region of retention time ranging from 66 to 85 min. (**c**) Dependence of HPLC peak intensity of fraction **A** on the Dy:[CN] molar ratio.

Table S1. Estimation of the relative yields of DyCN@C_{82}(C_2(5), C_s(6), C_{2v}(9)) to that of Dy_3N@C_{80} obtained from different extracts.

Extract (fraction)	Dy_2O_3/N_2 (fraction **A**)	Dy_2O_3/ $Fe_4[Fe(CN)_6]_3$ (fraction **A**)	Dy_2O_3/ $K_3[Fe(CN)_6]$ (fraction **A**)	Dy_2O_3/ $K_4[Fe(CN)_6]$ (fraction **A**)
Integrated area of fraction **A-1** (C_{86})	137.16	662.57	649.37	411.30
Integrated area of fraction **A-2**+**A-3**+**A-4**+**A-5** (DyCN@C_{2n} (2n=76, 82)	31.53	88.99	76.24	58.50
Integrated area of fraction **A-6** (Dy_3N@C_{80})	80.12	175.31	165.58	107.09
Relative yield of fraction **A-2**+**A-3**+**A-4**+**A-5** to Dy_3N@C_{80}	39.4%	50.8%	46.0%	54.6%
Integrated area of fraction **A-3** (DyCN@C_2(5)-C_{82})	17.37	51.19	49.90	35.92
Relative yield of fraction A-3 to **A-2**+**A-3**+**A-4**+**A-5**	55.1%	57.5%	65.5%	61.4%
Relative yield of fraction A-3 (DyCN@C_2(5)-C_{82}) to Dy_3N@C_{80}	**21.7%**	**29.2%**	**30.1%**	**33.5%**
Integrated area of fraction **A-4** (DyCN@C_s(6)-C_{82})	8.49	26.41	26.08	18.21
Relative yield of fraction **A-4** to **A-2**+**A-3**+**A-4**+**A-5**	26.9%	29.7%	34.2%	31.1%
Relative yield of fraction **A-4** (DyCN@C_s(6)-C_{82}) to Dy_3N@C_{80}	**10.6%**	**15.1%**	**15.7%**	**17.0%**
Integrated area of fraction **A-5** (DyCN@C_{2v}(9)-C_{82})	11.33	42.06	34.60	29.17
Relative yield of fraction **A-5** to **A-2**+**A-3**+**A-4**+**A-5**	35.9%	47.3%	45.4%	49.9%
Relative yield of fraction **A-5-3** to **A-5**	70.2%	70.2%	70.2%	70.2%
Relative yield of fraction **A-5-3** (DyCN@C_{2v}(9)-C_{82}) to Dy_3N@C_{80}	**9.9%**	**16.8%**	**14.7%**	**19.1%**

Given that the yield is proportional to the integrated area of HPLC peak of the corresponding fraction, the relative yields of DyCN@C_{82} (C_2(5), C_s(6), C_{2v}(9)) to $Dy_3N@C_{80}$ obtained from $Dy_2O_3/Fe_4[Fe(CN)_6]_3$ extract can be calculated as:

DyCN@C_2(5)-C_{82} : $Dy_3N@C_{80}$=51.19/175.31×100%=29.2%

DyCN@C_s(6)-C_{82} : $Dy_3N@C_{80}$=26.41/175.31×100%=15.1%

DyCN@C_{2v}(9)-C_{82} : $Dy_3N@C_{80}$=42.06/175.31×70.2%×100%=16.8%

Table S2. The relative yields and retention times of DyCN@C_{82}(C_2(5), C_s(6), C_{2v}(9)).

Extract (fraction)		DyCN@C_2(5)-C_{82} **(A-3)**	DyCN@C_s(6)-C_{82} **(A-4)**	DyCN@C_{2v}(9)-C_{82} **(A-5)**
Isomer label		I	II	III
Retention time (t_{ret}/min)		22.63-26.86	25.46-29.56	26.37-30.82
Relative yield	Dy_2O_3/N_2	21.7%	10.6%	9.9%
	Dy_2O_3/ $Fe_4[Fe(CN)_6]_3$	29.2%	15.1%	16.8%
	Dy_2O_3/ $K_3[Fe(CN)_6]$	30.1%	15.7%	14.7%
	Dy_2O_3/ $K_4[Fe(CN)_6]$	34.1%	17.0%	19.1%

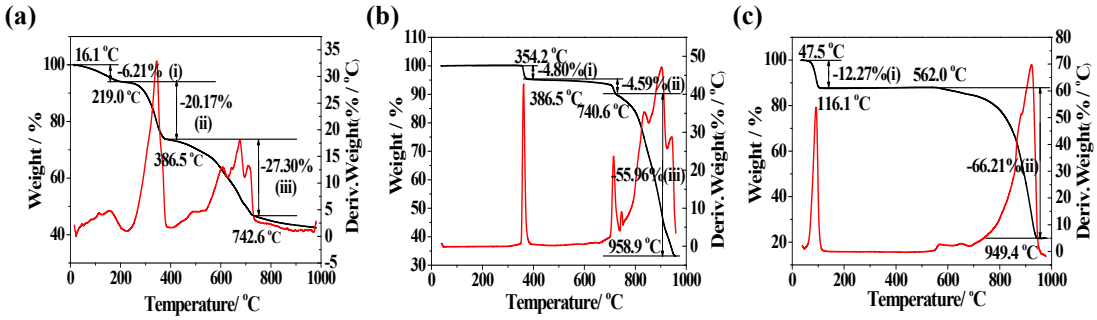

Fig. S3. TGA curves of (a) $Fe_4[Fe(CN)_6]_3$, (b) $K_3[Fe(CN)_6]$ and (c) $K_4[Fe(CN)_6]$. The temperature increase rate for all measurements was 10.00 ºC/min.

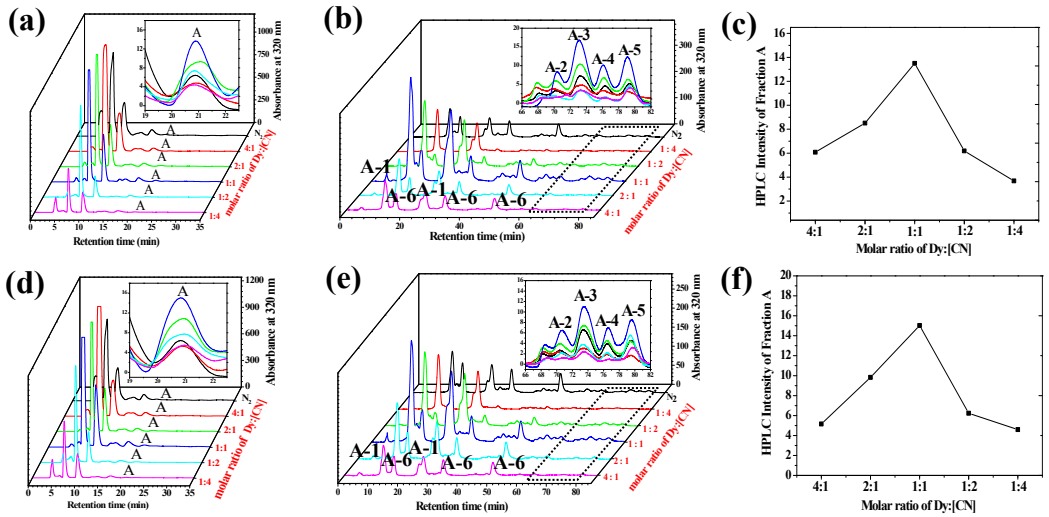

Fig. S4. HPLC chromatograms of $Dy_2O_3/K_3[Fe(CN)_6]$ and $Dy_2O_3/K_4[Fe(CN)_6]$ extracts with different Dy:[CN] molar ratios and HPLC intensity of fraction A. (**a, d**) HPLC chromatograms of the $Dy_2O_3/K_3[Fe(CN)_6]$ **(a)** and $Dy_2O_3/K_4[Fe(CN)_6]$ **(d)** extracts with different molar ratio (20 mm×250 mm 5PYE column; flow rate 15.0 mLmin^{-1}; injection volume 15 mL; toluene as the eluent (mobile phase); 40^{o}C). (**b, e**) Recycling HPLC chromatograms of fraction **A** obtained from $Dy_2O_3/K_3[Fe(CN)_6]$ (**b**) and $Dy_2O_3/K_4[Fe(CN)_6]$ (**e**) extracts with different Dy:[CN] molar ratios (10 mm×250 mm BPM column; flow rate 5.0 mL min^{-1}; injection volume 5 mL; toluene as the eluent (mobile phase); 40 ^{o}C). The dotted rhombus marks the enlarged region containing subfractions **A-2** to **A-6** shown in the inset of Fig. 2c. Inset: the enlarged region of retention time ranging from 66 to 85 min. (**c, f**) Dependence of HPLC peak intensity of fraction **A** obtained from $Dy_2O_3/K_3[Fe(CN)_6]$ (**c**) and $Dy_2O_3/K_4[Fe(CN)_6]$ (**f**) extracts on the Dy:[CN] molar ratio.

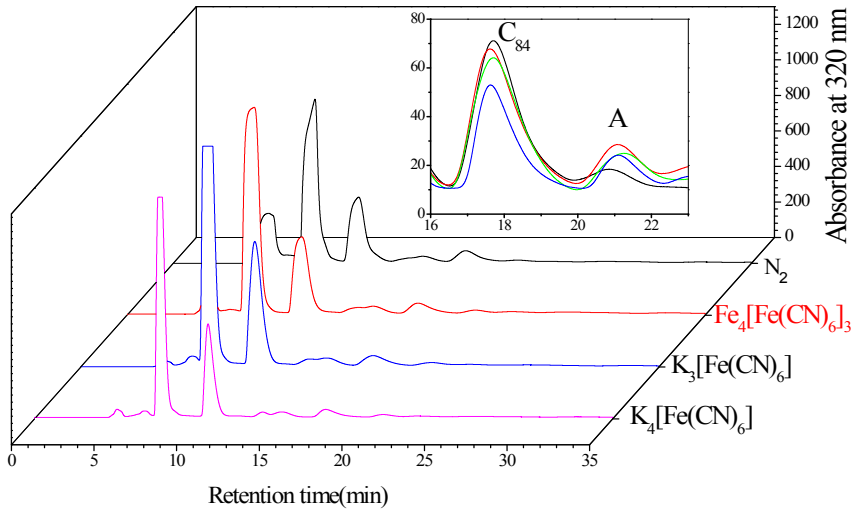

Fig. S5. HPLC chromatograms of the Dy_2O_3/N_2, $Dy_2O_3/Fe_4[Fe(CN)_6]_3$, $Dy_2O_3/K_3[Fe(CN)_6]$ and $Dy_2O_3/K_4[Fe(CN)_6]$ extracts obtained under optimized conditions (20 mm×250 mm 5PYE column; flow rate 15.0 mL min^{-1}; injection volume 15 mL; toluene as the eluent (mobile phase);

40 °C).

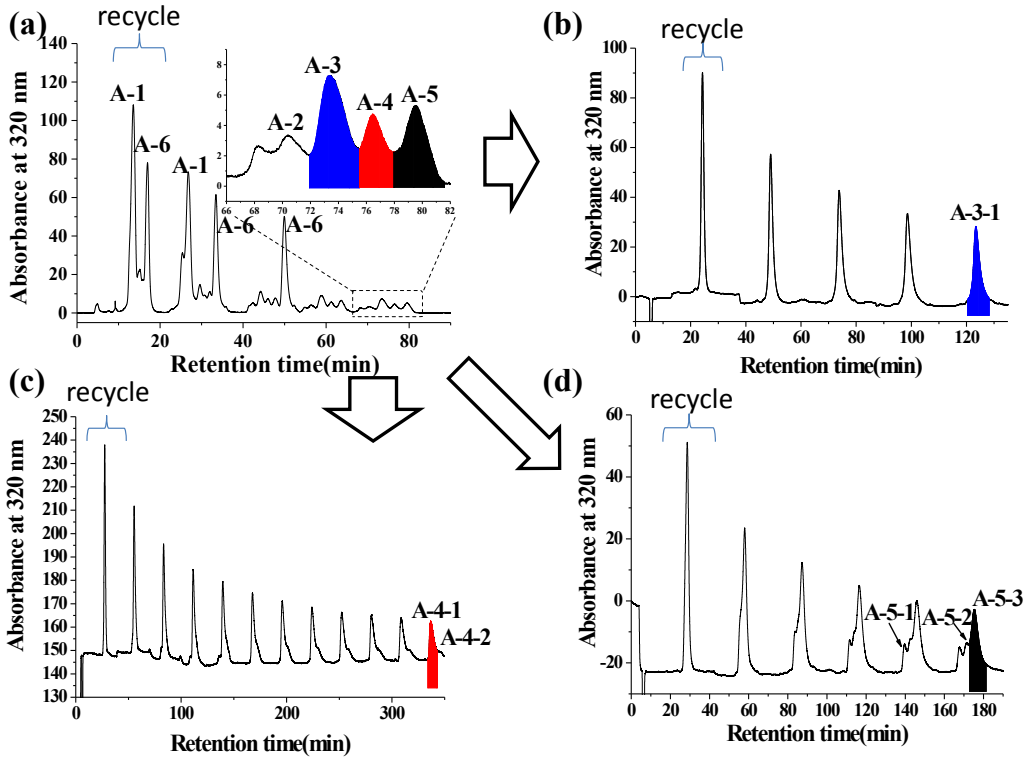

Fig. S6. Isolation scheme of DyCN@C_{82} (I-III). (**a**) Recycling HPLC chromatogram of fraction **A** isolated from the $Dy_2O_3/Fe_4[Fe(CN)_6]_3$ extract (10 × 250 mm Buckyprep-M column; flow rate 5.0 ml min^{-1}; injection volume 5 ml; toluene as eluent; 40°C). The inset shows the enlarged region of retention time ranging from 66 to 82 min. Subfractions **A-1**, **A-2**, **A-3, A-4, A-5, A-6** correspond to C_{86}, DyCN@C_{76}, DyCN@C_{82} (I), DyCN@C_{82} (II), DyCN@C_{82} (III), Dy_3N@C_{80} respectively. **A-1** and **A-6** were collected during the second and third cycles respectively. Copied from Fig. 2c. (**b-d**) Recycling HPLC chromatogram of fractions **A-3**, **A-4**, **A-5** (20 × 250 mm Buckyprep-M column; flow rate 15.0 ml/min; injection volume 15 ml; toluene as eluent; 40°C). **A-3-1**, **A-4-1** and **A-5-3** contains DyCN@C_{82} (I), DyCN@C_{82} (II) and DyCN@C_{82} (III), respectively.

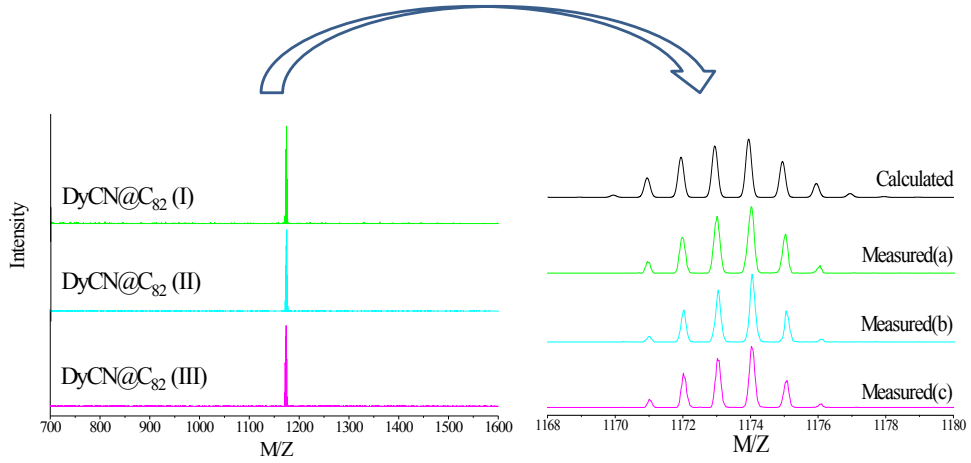

Fig. S7. MALDI-TOF mass spectra of the purified DyCN@C_{82} (I–III) in negative-ion mode.

Insets: the measured and calculated isotopic distributions.

S2. Thermal decomposition mechanism of $K_3[Fe(CN)_6]$ and $K_4[Fe(CN)_6]$.

Scheme S1. Possible decomposition processes of $K_3[Fe(CN)_6]$ and $K_4[Fe(CN)_6]$ during DC-arc discharge process.

1） Thermal decomposition of $K_3[Fe(CN)_6]$:

$$K_3[Fe(CN)_6]\bullet H_2O \rightarrow K_3[Fe(CN)_6] + H_2O\uparrow$$

(1)

$$24K_3[Fe(CN)_6] \rightarrow 18K_4[Fe(CN)_6] + 2Fe_3C + N_2\uparrow + 17(CN)_2\uparrow$$

(2)

$$3K_4[Fe(CN)_6] \rightarrow 12KCN + Fe_3C + 5C + 3N_2\uparrow$$

(3)

$$KCN + H_2O \rightarrow KOH + HCN\uparrow$$

(4)

$$2KOH \rightarrow K_2O + H_2O\uparrow$$

(5)

$$24K_3[Fe(CN)_6]\bullet H_2O \rightarrow 8Fe_3C + 30C + 24K_2O + 24KCN + 17(CN)_2\uparrow + 19N_2\uparrow + 48HCN\uparrow$$

(6)

2） Thermal decomposition of $K_4[Fe(CN)_6]$:

$$K_4[Fe(CN)_6]\bullet 3H_2O \rightarrow K_4[Fe(CN)_6] + 3H_2O\uparrow$$

(7)

$$3K_4[Fe(CN)_6] \rightarrow 12KCN + Fe_3C + 5C + 3N_2\uparrow$$

(8)

$$KCN + H_2O \rightarrow KOH + HCN\uparrow$$

(9)

$$2KOH \rightarrow K_2O + H_2O\uparrow$$

(10)

$$6K_4[Fe(CN)_6]\bullet 3H_2O \rightarrow 2Fe_3C + 10C + 12K_2O + 12HCN\uparrow + 6N_2\uparrow + 6H_2O\uparrow$$

(11)

S3. X-ray crystallographic analysis of DyCN@C_{82} (C_2(5), C_s(6), C_{2v}(9)).

Table S3. Crystal data and data collection parameters.

Crystal	DyCN@C_2(5)-C_{82}·2(DPC)·3(C_7H_8)	DyCN@C_s(6)-C_{82}·2(DPC)·4(C_7H_8)	DyCN@C_{2v}(9)-C_{82}·2(DPC)·4(C_7H_8)
Formula weight	3251.78	3343.91	3343.77
Wavelength(λ, Å)	0.77488	0.77488	0.77488
Temperature/K	100(2)	100(2)	100(2)
Crystal system	monoclinic	monoclinic	monoclinic
Space group	$P2_1/c$	$P2_1/c$	$P2_1/c$
a, Å	14.84	14.69	14.703
b, Å	32.001	32.116	32.003
c, Å	32.602	32.24	32.227
α, deg	90	90	90
β, deg	102.65	101.86	101.7
γ, deg	90	90	90
Volume, Å^3	15106.7	14885.618	14849.028
Z	4	4	4
Unique data(R_{int})	27442(0.056)	32714(0.146)	31171(0.114)
Parameters	2270	3221	2492
Restraints	1084	2633	478
Observed data(I>2σ(I))	24190	28143	23346
$R1^a$ (observed)	0.1087	0.0809	0.0905
$wR2^b$(all data)	0.3232	0.2443	0.2782

[a]For data with I>2σ(I), RI=1||F_o|-| F_c||/Σ |F_o|. [b]For all data, wR2={Σ[w(F_o^2-F_c^2)^2])/ Σ[w(F_o^2)^2]}$^{1/2}$.

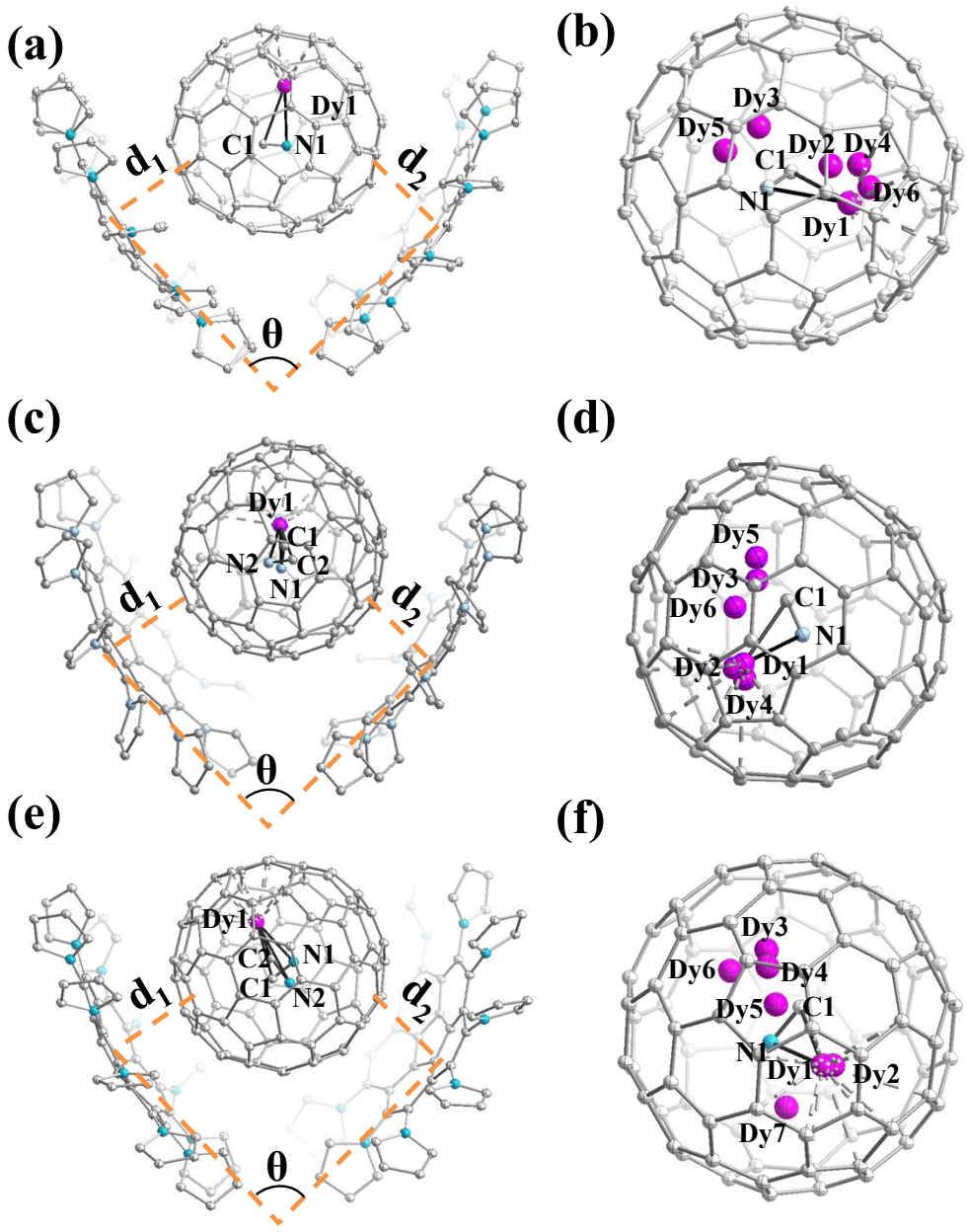

Fig. S8. Single crystal X-ray structures of DyCN@C_{82} (C_2(5), C_s(6), C_{2v}(9)) showing all Dy sites. All solvent toluene molecules and hydrogen atoms are omitted for clarity. (**a**) Structure of DyCN@C_2(5)-C_{82}·2(DPC) with only one predominant Dy (Dy1) and all Dy sites (**b**), of which the fractional occupancies are 0.4161(15), 0.1556(18), 0.1537(18), 0.138(3), 0.0758(11), and 0.061(3) for Dy1, Dy2, Dy3, Dy4, Dy5 and Dy6, respectively. (**c**) Structure of DyCN@C_s(6)-C_{82}·2(DPC) with two CN group disorders (the fractional occupancies are 0.65 and 0.35 for C1-N1 and C2-N2 groups, respectively), one predominant Dy (Dy1) and all Dy sites (**d**), of which the fractional occupancies are 0.369(3), 0.181(3), 0.146(2), 0.127(3), 0.0896(15) and 0.087(2) for Dy1, Dy2, Dy3, Dy4, Dy5 and Dy6, respectively. (**e**) Structure of DyCN@C_{2v}(9)-C_{82}·2(DPC) with two CN group disorders (the fractional occupancies are 0.53 and 0.47 for C1-N1 and C2-N2 groups, respectively), one predominant Dy (Dy1) and all Dy sites (**d**), of which the fractional occupancies are 0.376(3), 0.172(3), 0.127(3), 0.098(3), 0.089(2) , 0.0703(18) and 0.0674(11) for Dy1, Dy2,

Dy3, Dy4, Dy5, Dy6 and Dy7, respectively.

Table S4. The geometric structures parameters of DyCN@C_{82}(C_2(5), C_s(6), C_{2v}(9)) and DPC.

Endohedral fullerenes	θ/°	d_1/Å	d_2/Å
DyCN@C_2(5)-C_{82}	67.15	3.33	3.30
DyCN@C_s(6)-C_{82}	65.16	3.28	3.29
DyCN@C_{2v}(9)-C_{82}	65.57	3.31	3.30

S4. UV-vis-NIR spectroscopic data of DyCN@C_{82} (C_2(5), C_s(6), C_{2v}(9)).

Table S5.Characteristic absorption data of DyCN@C_{82}(C_2(5), C_s(6), C_{2v}(9)). Other analogous C_{82}-based endohedral fullerenes were also listed for comparison.

Endohedral fullerene	Absorption peaks (nm)	λ_{onset} (nm)	$\Delta E_{gap,\ optical}$ (eV) [a]	Ref.
DyCN@C_2(5)-C_{82}	630, 657, 769, 933, 1069	1261	0.98	This work
TbCN@C_2(5)-C_{82}	392, 627, 656, 763, 923, 1056	1240	1.00	21
LuCN@C_2(5)-C_{82}	631, 662, 764, 941, 1062	1242	1.00	23
Yb@C_2(5)-C_{82}	500, 650, 780, 1020, 1180	1350	0.92	34
Eu@C_2(5)-C_{82}	490, 640, 790, 1020, 1190	1360	0.90	35
DyCN@C_s(6)-C_{82}	497, 744, 1024, 1140, 1339	1656	0.75	This work
TbCN@C_s(6)-C_{82}	491, 744, 1072, 1132, 1318	1620	0.77	21
LuCN@C_s(6)-C_{82}	494,596, 744, 1069, 1131, 1345	1638	0.76	23
Yb@C_s(6)-C_{82}	800, 880, 1220, 1450	1850	0.67	34
DyCN@C_{2v}(9)-C_{82}	536, 627, 1144, 1342	1785	0.69	This work
TbCN@C_{2v}(9)-C_{82}	518, 618, 710, 772, 1144, 1320	1770	0.70	21
LuCN@C_{2v}(9)-C_{82}	512, 621, 697, 782, 1096, 1296	1680	0.74	23
Yb@C_{2v}(9)-C_{82}	480, 800, 1160, 1500	1850	0.67	34

[a] $\Delta E_{gap,\ optical} = 1240 / \lambda_{onset}$.

S5. Cyclic voltammograms of DyCN@C_{82} (C_2(5), C_s(6), C_{2v}(9)) in different scanning regions.

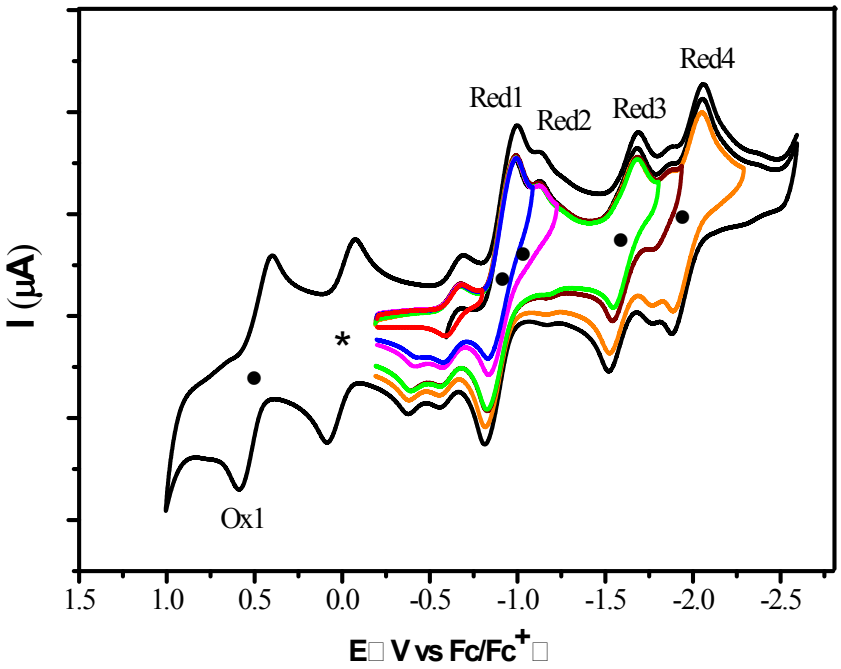

Fig. S9. Cyclic voltammograms of DyCN@C_2(5)-C_{82} measured in *o*-DCB solution in different scanning regions showing the correlation of each reduction step with the corresponding re-oxidation step. Scan rate: 100 mV·s^{-1}, $TBAPF_6$ as supporting electrolyte. Each redox step is marked with a number and a solid dot to aid comparison. The asterisk labels the oxidation peak of ferrocene.

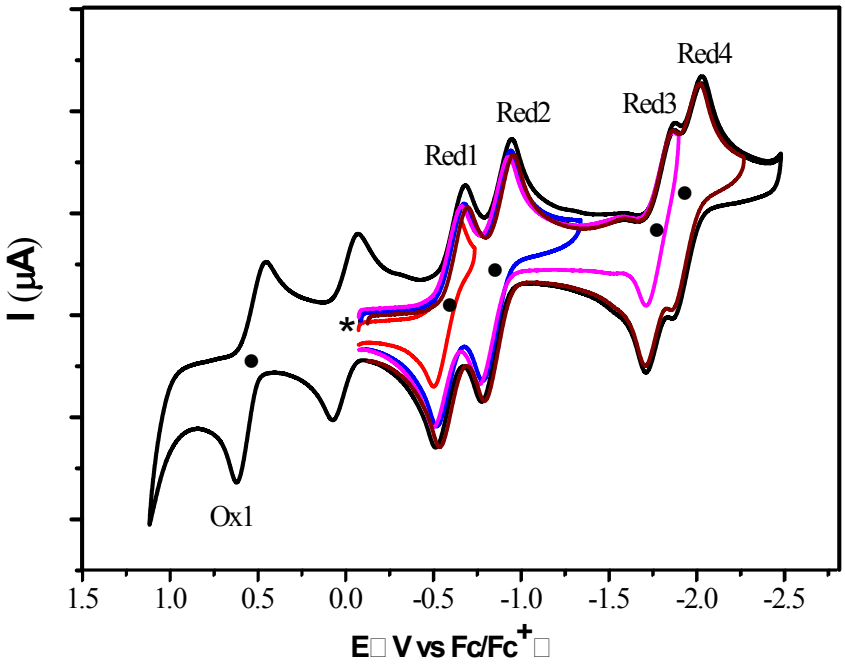

Fig. S10. Cyclic voltammograms of DyCN@*C*s (6)-C_{82} measured in o-DCB solution in different scanning regions showing the correlation of each reduction step with the corresponding re-oxidation step. Scan rate: 100 $mV \cdot s^{-1}$, $TBAPF_6$ as supporting electrolyte. Each redox step is marked with a number and a solid dot to aid comparison. The asterisk labels the oxidation peak of ferrocene.

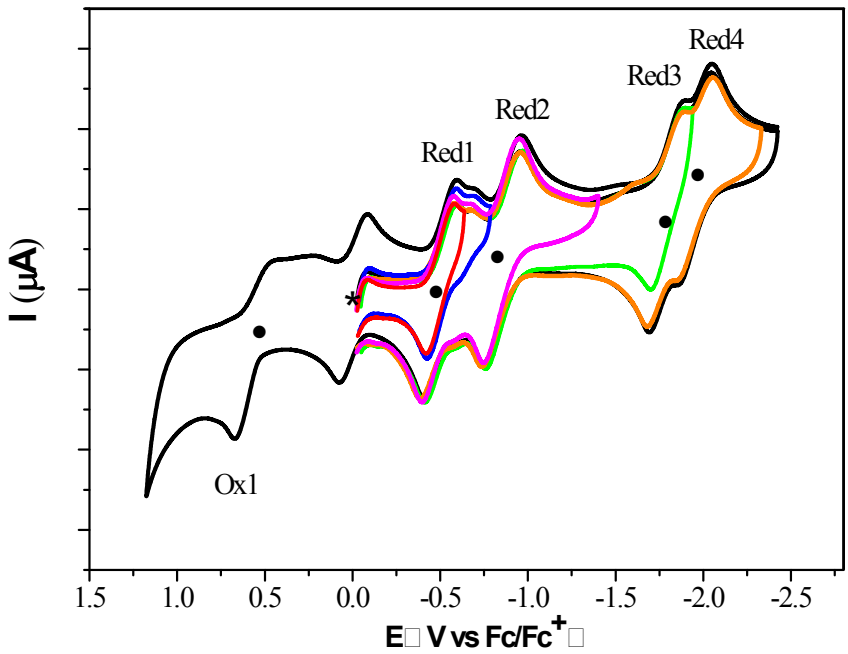

Fig. S11. Cyclic voltammograms of DyCN@C_{2v}(9)-C_{82} measured in o-DCB solution in different scanning regions showing the correlation of each reduction step with the corresponding re-oxidation step. Scan rate: 100 $mV \cdot s^{-1}$, $TBAPF_6$ as supporting electrolyte. Each redox step is marked with a number and a solid dot to aid comparison. The asterisk labels the oxidation peak of ferrocene.